Altered Thermodynamics from Remote Mutations Altering Human toward Bovine Purine Nucleoside Phosphorylase†

Mahmoud Ghanem, Lei Li, Corin Wing, and Vern L. Schramm*

Department of Biochemistry, Albert Einstein College of Medicine, 1300 Morris Park Avenue, Bronx, New York 10461

Received October 23, 2007; Revised Manuscript Received December 4, 2007

ABSTRACT: Human (HsPNP) and bovine (BtPNP) purine nucleoside phosphorylases are homotrimers with the catalytic sites located near the subunit−subunit interfaces. Despite the high amino acid sequence similarity (87% identical) and the fully conserved catalytic site contacts between BtPNP and HsPNP, crystal structures reveal that the subunits interact differently and isotope effect studies indicate distinct transition-state structures. The subunit interfaces and crystallographic packing properties of BtPNP differ from HsPNP. Hypothetically, mutating HsPNP toward BtPNP might alter the dynamic, catalytic and subunit packing properties of HsPNP to become more similar to BtPNP. Amino acids Lys22 and His104 in HsPNP were target candidates based on crystal packing contacts and were replaced with their BtPNP counterparts to give Lys22Glu:His104Arg (E:R-PNP). The kinetic properties (steady and pre-steady state), inhibition constants, and thermodynamic properties of E:R-PNP were compared to HsPNP and BtPNP. The E:R-PNP is similar to HsPNP in steady-state kinetic properties. However HsPNP and E:R-PNP show remarkable ratios for (K_m guanosine)/(K_i* DADMe-ImmG) of 2.8×10^7 and 4.7×10^7 respectively, suggesting that DADMe-ImmG is an excellent mimic of the transition states for both HsPNP and E:R-PNP with a preference for E:R-PNP. Thermodynamic parameters obtained from the temperature dependence studies of the chemical step establish E:R-PNP to be catalytically more efficient than the parent enzyme and reveal differences in the entropic component of catalysis. The two companion manuscripts (Luo, M., Li, L. and Schramm, V. L. (2008) *Biochemistry 47*, 2565−2576; Li, L., Luo, M., Ghanem, M., Taylor, E. A., and Schramm, V. L. (2008) *Biochemistry 47*, 2577−2583) report changes in transition-state structure as a consequence of mutations remote from the catalytic sites of both HsPNP and BtPNP.

Purine nucleoside phosphorylase (PNP, EC 2.4.2.1) catalyzes the reversible phosphorolysis of purine (deoxy)-ribonucleosides to the corresponding purine base and (2′-deoxy) ribose 1-phosphate (Figure 1) (*1*, *2*). The genetic deficiency of HsPNP[1] results in a specific T-cell immunodeficiency due to the accumulation of deoxyguanosine in blood and dGTP in activated, dividing T-cells (*3*). Inhibition of HsPNP provides a potential therapy for T-cell cancers and autoimmune diseases (*4*−*6*).

The first-generation transition state analogue inhibitors, immucillins (ImmH and ImmG) (Figure 2), were designed on the basis of an early ribooxacarbenium transition-state structure for BtPNP (*7*). Both inhibitors showed slow-onset, tight-binding competitive inhibition for both bovine and human enzymes, with preference for the bovine enzyme (*1*, *8*). ImmH has proven to be pharmacologically favorable and has entered phase II clinical trials for the treatment of T- and B-cell cancers (Forodesine) (*6*, *8*).

Despite the high amino acid sequence similarity (87% identical) and the fully conserved catalytic site contacts between BtPNP and HsPNP, ImmH binds to BtPNP 2.4-fold tighter than to HsPNP (K_i* values of 23 and 56 pM, respectively), suggesting dissimilarity of the transition-state structures between HsPNP and BtPNP (*1*, *9*, *10*). Consequently, the transition-state structure of HsPNP was solved, and showed a near-fully dissociated ribooxacarbenium ion transition state with full leaving-group departure prior to the nucleophilic attack of phosphate (*1*, *9*).

The second-generation DADMe-immucillin transition state analogue inhibitors (DADMe-ImmH and DADMe-ImmG) (Figure 2) were synthesized to mimic this fully dissociated transition state (*8*, *9*, *11*). This new generation of transition state analogue inhibitors was superior in inhibiting HsPNP with K_i* values of 16 and 7 pM for DADMe-ImmH and DADMe-ImmG, respectively (*1*, *8*). DADMe-ImmH was called "the ultimate inhibitor" for mouse PNP due to its ability to inhibit the enzyme *in vivo* for the lifetime of erythrocytes following a single oral administration (*11*). DADMe-ImmH has entered phase II clinical trials for autoimmune disease indications under the names BCX-4208 and R3421 (*1*).

Human and bovine PNPs are homotrimers, and the catalytic sites are located near the subunit−subunit interface. The catalytic sites consist of residues N243, E201, H257, F200, Y88, M219, and F159 as contacts for the nucleoside, and residues S33, H64 (in BtPNP only), R84, H86, A116,

† Supported by NIH Research Grants GM41916 and GM068036.

* Author to whom correspondence should be addressed. E-mail: vern@aecom.yu.edu. Tel: (718) 430-2813. Fax: 718-430-8565.

[1] Abbreviations: HsPNP and BtPNP, human and bovine purine nucleoside phosphorylases, respectively; E:R-PNP, mutated form of human PNP in which Lys22 and His104 are substituted with Glu and Arg, respectively (K22E and H104R); DADMe-ImmH, 4′-deaza-1′-aza-2′-deoxy-1′-(9-methylene)-immucillin-H; ImmH, immucillin-H; DADMe-ImmG, 4′-deaza-1′-aza-2′-deoxy-1′-(9-methylene)-immucillin-G; ImmG, immucillin-G.

10.1021/bi702132e CCC: $40.75
Published on Web 02/19/2008

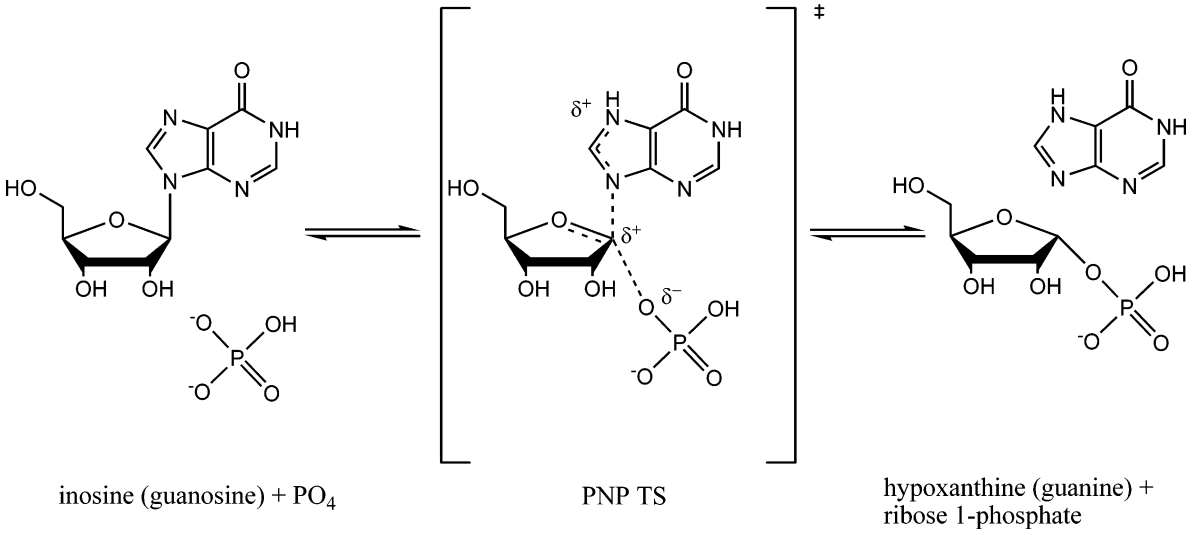

FIGURE 1: Phosphorolysis reaction of the conversion of purine nucleoside (inosine or guanosine) to purine base (hypoxanthine or guanine), catalyzed by PNP.

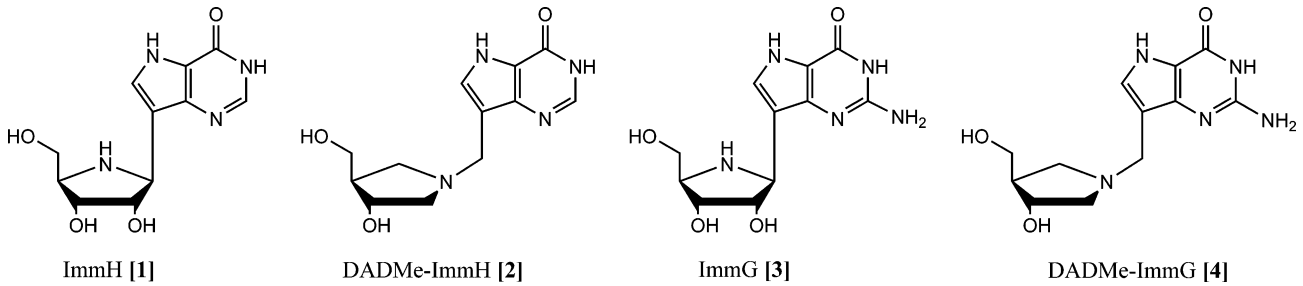

FIGURE 2: First- and second-generation transition-state analogues (immucillins) that mimic the transition state ribooxacarbenium ion character of PNPs.

and S220 as contacts for the phosphate group. In addition, two catalytic waters (WAT502 and WAT520) are buried in the catalytic site (*12*). F159 is a catalytic site residue from the adjacent subunit and covers the catalytic site from accessible solvent (*12*).

Based on the catalytic activity and the crystallographic packing properties of BtPNP compared to HsPNP, it was hypothesized that mutation of HsPNP toward BtPNP might improve the crystallographic properties of HsPNP to match the superior diffraction properties of BtPNP. It was also of interest to determine if mutations remote from the catalytic site, but involved in the overall architecture of the enzyme, would influence catalytic properties and transition-state structure. Amino acids Lys22 and His104 of HsPNP were selected as target candidates from electrostatic differences at crystal lattice contacts of the enzymes. The surface residues, Lys22 and His104 in HsPNP were replaced with Glu and Arg, respectively, to match the electrostatics for these BtPNP surface residues. The kinetic properties (steady state and pre-steady state), inhibition constants and structural properties of E:R-PNP were compared to human and bovine enzymes. The rate and thermodynamic properties of the catalytic step are altered by these mutations. The following papers demonstrate that remote or second-sphere mutations influence transition-state structure for both HsPNP and BtPNP. Finally, QM/MM calculations have been used to demonstrate that these mutations also change the dynamic properties at numerous sites throughout the protein and that these dynamic changes are transmitted into the catalytic site.[2]

MATERIALS AND METHODS

WT-Bovine PNP. Wild-type bovine PNP (BtPNP, calf spleen) in 3.2 M ammonium sulfate was purchased from Sigma.

Site-Directed Mutagenesis. Site-directed mutagenesis of the two residues (K22 and H104) was carried out using a QuikChange Multi Site-Directed Mutagenesis kit (Stratagene) to prepare the bovinized HsPNP (E:R-PNP), in which Lys22 and His104 were replaced with Glu and Arg, respectively. The method used was according to the manufacturer's instructions, using the native HsPNP cDNA inserted into pCRT7/NT-TOPO (*9*) as a template and K22Ef 5′-GCT-TCTGTCTCATACTGAGCAGCGACCTCAAGT-3′, K22Er 5′-ACTTGAGGTCGGTGCTCAGTATGAGCAAGAAC-3′, H104Rf 5′-AGTGAGGGTTTTCCGCCTTCTGGGT-GTGG-3′, H104Rr 5′-CCACACCCAGAAGGCGGAAAAC-CCTCACT-3′ oligonucleotides as forward (f) and reverse (r) primers (underlined letters indicate mismatches). The DNA sequence was confirmed by automated DNA sequencing, and the plasmid was transformed into *Escherichia coli* strain BL21(DE3)pLysS competent cells (Invitrogen).

Expression and Purification of HsPNP and E:R-PNP. HsPNP and E:R-PNP were expressed and purified to

[2] S. Saen-Oon, M. Ghanem, C. Wing, V. L. Schramm, and S. D. Schwartz, (2008) *Biophys. J. 94*, in press.

homogeneity as judged by SDS−PAGE using the same procedure used previously for the purification of the native HsPNP (*9*).

Enzymes Assays. Activity assays for HsPNP, E:R-PNP, and the BtPNP with inosine as a substrate were carried out as previously described by monitoring the conversion of hypoxanthine to uric acid ($\epsilon_{293} = 12.9$ mM^{-1} cm^{-1}) (*13*) in a coupled assay containing 60 milliunits of xanthine oxidase and variable concentrations of inosine, in 50 mM KH_2PO_4, pH 7.4 at 25 °C (*11*). Activity assays for HsPNP, E:R-PNP, and BtPNP with guanosine were carried out by monitoring the formation of guanine ($\epsilon_{257} = -5.07$ mM^{-1} cm^{-1}) in direct assays containing variable concentrations of guanosine, in 50 mM KH_2PO_4, pH 7.4 at 25 °C.

Slow-Onset Inhibition. Slow onset inhibition was measured following the addition of enzyme to complete assay mixtures at 1 mM inosine and various inhibitor concentrations (*14*, *15*). Inhibitor concentrations were determined spectrophotometrically using the published millimolar extinction coefficients of 9.54 at 261 nm and 8.92 at 269 nm at pH 7 for 9-deazainosine (ImmH based inhibitors) and 9-deazaguanosine (ImmG based inhibitors), respectively (*10*, *15*, *16*). Enzyme (0.2−0.5 nM final concentration) was added to assay mixtures followed by monitoring of product formation. Rates were monitored for 1−2 h to determine the initial reaction rate and to determine if a second reaction rate occurred as a result of slow-onset inhibition. The inhibition constant (K_i) for the initial rate was determined from its fit to eq 1, which

$$\frac{v}{e} = \frac{k_{cat}A}{K_m\left(1 + \frac{Imm}{K_i}\right) + A} \quad (1)$$

describes the competitive inhibition pattern of the immucillin based inhibitors (Imm) and inosine as substrate (A). K_m is the Michaelis constant for inosine (A), and K_i is the dissociation constant of inhibitor from the PNP·PO_4 complex, assuming competitive inhibition. The dissociation constant for the equilibrium complex after slow-onset inhibition has occurred, K_i*, was determined from fits of the final slopes to eq 1 (*15*).[3]

Stopped-Flow Fluorescence Kinetics. The temperature dependence of single turnover catalysis with guanosine was determined using an Applied Photophysics stopped-flow spectrophotometer (model π*-180 spectrometer) equipped with a thermostated water bath. The fluorescence increase caused by enzyme-bound guanine was followed by excitation at 280 nm and emission above 290 nm (2.5 nm slit widths, 2 mm path length). The rates (k_3) represent the conversion of PNP·guanosine·PO_4 to PNP·guanine·R-1-P (Figure 3). Equal volumes of ~4 μM enzyme in 50 mM KH_2PO_4 pH 7.4 were rapidly mixed with saturated guanosine (~2 mM) in the same buffer. The temperature was varied from 4 to 20 °C. Two hundred data points were collected over 0.1 to 0.5 s, and at least 3 runs were averaged at each temperature.

[3] Origin of K_i and K_i* based on the slow-onset tight-binding of immucillins (Imm):

$$PNP{\cdot}PO_4 + Imm \underset{k_2}{\overset{k_1}{\rightleftharpoons}} PNP{\cdot}Imm{\cdot}PO_4 \underset{k_4}{\overset{k_3}{\rightleftharpoons}} PNP^*{\cdot}Imm{\cdot}PO_4$$

$$K_i = k_2/k_1$$

$$K_i^* = K_i(k_4/k_3 + k_4)$$

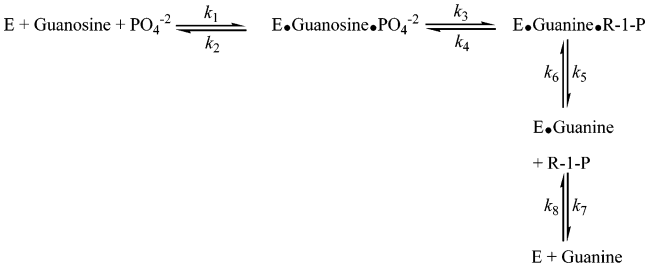

FIGURE 3: The reaction scheme of PNP (E) for conversion of guanosine to guanine and ribose 1-phosphate (R-1-P). Only the enzyme-bound guanine is fluorescent under these conditions. Product release is rate-limiting.

The single turnover rates at different temperatures were determined by fitting the stopped-flow traces into the equation for single-exponential decay (eq 2), where k_{obs} represents the first-order rate constant of the chemical step (k_3), t is time, F_t is the fluorescence emission intensity above 290 nm, A is the amplitude of the total change, and F_∞ is the fluorescence intensity at infinite time.

$$F_t = A\exp(-k_{obs}t) + F_\infty \quad (2)$$

The temperature dependence of the single turnover rates (k) were determined by fitting the data with the Arrhenius and the Eyring equations (eqs 3 and 4, respectively), where k_B and h are the Boltzmann and Planck constants, respectively, A is the preexponential factor, E_a is the energy of activation, R is the gas constant (8.31 J mol^{-1} K^{-1}), and T is the temperature in kelvins. The enthalpy of activation ($\Delta H^\ddagger$) is calculated from the slope of the plots, whereas the entropy ($\Delta S^\ddagger$) is calculated from y-intercept of the plots.

$$\ln(k) = \ln A - [E_a/RT] \quad (3)$$

$$\ln(k/T) = \ln(k_B/h) + \Delta S^\ddagger/R - \Delta H^\ddagger/RT \quad (4)$$

RESULTS AND DISCUSSION

Expression and Purification of E:R-PNP. HsPNP and E:R-PNP were expressed and purified to homogeneity as judged by SDS−PAGE using the procedure described previously for the purification of the native HsPNP (*9*). Approximately 80−100 mg of purified E:R-PNP was typically obtained from cells cultured in one liter of Luria−Bertani culture medium.

Steady-State Kinetic Properties. The steady-state kinetic parameters of HsPNP, E:R-PNP, and BtPNP were determined with either inosine or guanosine as substrates (Table 1). E:R-PNP is catalytically similar to HsPNP and BtPNP in converting inosine or guanosine to hypoxanthine or guanine, respectively, and ribose 1-phosphate (Table 1). Although the catalytic efficiency (k_{cat}/K_m) of all three enzymes was similar, k_{cat} and K_m values of HsPNP with inosine as substrate were greater than those of BtPNP (Table 1). Tighter binding of substrate/product correlating with slower turnover numbers (k_{cat}) is found when product release is a rate-limiting step in steady-state catalysis. The k_{cat} and K_m values for E:R-PNP with inosine as substrate were between those for human and bovine enzymes but were closer to those for HsPNP (Table 1). Since the three PNPs are similar in catalytic efficiency (k_{cat}/K_m) and the rate-limiting step of some PNPs is known to be release of purine

Table 1: Comparison of Steady-State Kinetic Constants for HsPNP, E:R-PNP and BtPNP with Either Inosine or Guanosine as Substrate[a]

parameter	HsPNP	E:R−PNP	BtPNP
	Inosine as a Substrate		
k_{cat}, s^{-1}	40 ± 1	31.5 ± 0.5	20 ± 1
K_m, μM	30 ± 2	27 ± 2	16 ± 1
k_{cat}/K_m, M^{-1} s^{-1}	(1.3 ± 0.1) × 10^6	(1.2 ± 0.1) × 10^6	(1.25 ± 0.1) × 10^6
	Guanosine as a Substrate		
k_{cat}, s^{-1}	31 ± 2	30 ± 2	27 ± 1
K_m, μM	42 ± 7	47 ± 7	49 ± 6
k_{cat}/K_m, M^{-1} s^{-1}	(0.73 ± 0.13) × 10^6	(0.63 ± 0.10) × 10^6	(0.55 ± 0.07) × 10^6

[a] Enzymatic activity was measured in 50 mM KH_2PO_4, pH 7.4, at 25 °C.

(*1*), BtPNP might be expected to exhibit the highest chemical rate (single turnover number) followed by E:R-PNP and HsPNP.

Slow-Onset Inhibition of E:R-PNP. The second-generation transition-state inhibitors, DADMe-ImmH [**2**] and DADMe-ImmG [**4**], are powerful inhibitors for E:R-PNP and bind tightly with K_i* values of 15 and 1 pM, respectively, compared to K_i* values of 85 and 7 pM for first-generation inhibitors (ImmH and ImmG, respectively) (Table 2). The binding of DADMe-ImmG to E:R-PNP is remarkable by giving a ratio of 47,000,000 for (K_m guanosine)/(K_i* DADMe-ImmG), the highest binding affinity for any transition-state analogue with any known PNP.

The pattern of selective inhibition by the DADMe-immucillins relative to immucillins is also observed for both E:R-PNP and HsPNP (Table 2), suggesting a transition-state structure for E:R-PNP more similar to that of HsPNP. In contrast, BtPNP shows strong selectivity for ImmH [**1**] relative to DADMe-ImmH [**2**] with K_i* values of 23 and 100 pM for ImmH and DADMe-ImmH, respectively (*17*, *18*). The binding preference of BtPNP for [**1**] and [**2**] reverses with the 9-deazaguanine-based inhibitors, ImmG [**3**] and DADMe-ImmG [**4**], where the K_i* values were 55 and 14 pM, respectively. Discrimination of BtPNP binding to immucillin-H or immucillin-G based inhibitors is consistent with the K_m values of inosine compared to guanosine substrates (K_m values of 16 μM and 49 μM, respectively) (Tables 1 and 2). Therefore, using inosine as substrate and immucillin-H based inhibitors provides the more reliable probe for transition-state structure of these PNPs.

Transition-State Structure of E:R-PNP. Despite the 87% amino acid sequence identity between HsPNP and BtPNP, their transition-state structures differ substantially. BtPNP has an early ribooxacarbenium ion transition-state structure featuring a C1′−N9 bond of approximately 1.8 Å (*7*). In contrast, HsPNP has a near-fully dissociated transition state, in which the leaving group (hypoxanthine) departure is

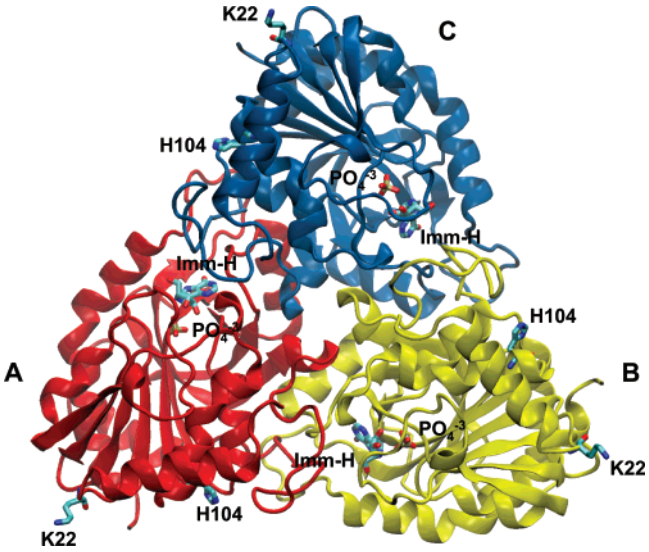

FIGURE 4: Trimeric crystal structure of HSPNP in complex with Immucillin-H (Imm-H) and phosphate (PDB IRR6).

complete (3.0 Å) prior to the nucleophilic group (arsenate) attack, and the ribosyl group is a fully developed ribooxacarbenium ion (*1*, *8*, *9*). If mutation of the remote H:R residues influences transition-state structure, the TS for E:R-PNP would be expected to be different from HsPNP and BtPNP. This is the case, as described in a companion paper (*34*).

Pre-Steady-State Kinetics. The chemical step of C1′−N9 bond cleavage and formation of enzyme-bound products is faster for E:R-PNP than for HsPNP (Table 3). With chemical steps of 154 and 214 s^{-1}, and steady-state k_{cat} values of 30 and 31 s^{-1} for guanosine phosphorolysis, guanine release is implicated as the overall rate-limiting step for both HsPNP and H:R-PNP. This reaction pathway for E:R-PNP is also supported by the comparative principal component or Essential Dynamics analysis comparing HsPNP and E:R-PNP.[2] The enzymes complexed with ImmG and phosphate show correlated motions between the phosphate loop (residues 57−65; subunit A) and the F159 loop (residues 155−160; subunit

Table 3: Comparison of the Thermodynamic Parameters of HsPNP, E:R-PNP and BtPNP for Phosphorolysis of Guanosine

parameter	HsPNP	E:R−PNP	BtPNP
k_3, s^{-1} (25 °C)[a]	154 ± 3	214 ± 3	316 ± 6
k_3, s^{-1} (37 °C)[a]	540 ± 15	840 ± 90	942 ± 176
$T\Delta S^{\ddagger}$,[b] kJ mol^{-1}	17 ± 1	25 ± 1	9.0 ± 0.5
$\Delta H^{\ddagger}$,[c] kJ mol^{-1}	78 ± 3	85 ± 3	67 ± 3
E_a,[d] kJ mol^{-1}	80 ± 3	87 ± 3	70 ± 3
$\Delta G^{\ddagger}$,[b] kJ mol^{-1}	60 ± 4	60 ± 4	58 ± 3

[a] Rates for 25 and 37 °C were obtained by extrapolating the stopped-flow fluorescence rates using the Arrhenius equation (eq 3). [b] Data for 25 °C. [c] Data were calculated by using the Eyring equation (eq 4).[d] Data were calculated by using the Arrhenius equation (eq 3)

Table 2: Comparison of the Inhibition Constants (K_i and K_i*) of HsPNP, E:R-PNP and BtPNP for Selected Immucillin Based Inhibitors

	HsPNP		E:R−PNP		BtPNP	
inhibitor	K_i (pM)	K_i* (pM)	K_i (pM)	K_i* (pM)	K_i (pM)	K_i* (pM)
ImmH [**1**]	>1000	88 ± 3	670 ± 40	85 ± 6	~41,000[a]	23[b]
DADMe-ImmH [**2**]	350 ± 60	8.5 ± 0.2	240 ± 60	15 ± 1	>1000	100[c]
ImmG [**3**]	133 ± 21	9.2 ± 0.1	175 ± 30	7.0 ± 0.2	463 ± 75	55 ± 4
DADMe-ImmG [**4**]	34 ± 4	1.5 ± 0.1	121 ± 7	1.0 ± 0.1	454 ± 100	14 ± 3

[a] From (*10*). [b] From (*17*). [c] From (*18*).

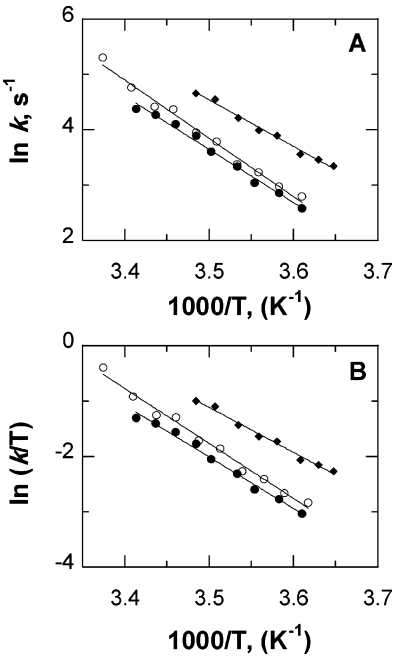

FIGURE 5: Arrhenius (panel A) and Eyring (panel B) plots for the temperature dependences of the single turnover rates (k_3) for HsPNP (●), E:R-PNP (○), and BtPNP (◆). The rates of fluorescence increase due to the formation of PNP•guanine•R-1-P were recorded in the temperature range from 1 to 20 °C. Data were fit to eqs 3 and 4 as indicated in Materials and Methods.

C).[2] Overall, the longer side chain of Arg104 enhances the mobility and the dynamics of the F159 loop of subunit C which in turn enhances the geometry and the dynamics of the residues that form a hydrophobic cluster around the substrate/transition-state analogue (H257, F200, and Y88; subunit A) and consequently stabilize the transition state ribooxacarbenium ion of E:R-PNP.

Thermodynamic Properties of PNPs. The temperature dependence of the catalytic step (k_3) for BtPNP, HsPNP and E:R-PNP was explored by single turnover kinetics (Figures 3 and 5, Table 3). Single-turnover rates were measured in the presence of near-saturating guanosine and phosphate by monitoring the increase of fluorescence intensity due to the formation of the PNP•guanine•R-1-P complexes (*19*, *20*). Guanine bound to PNP is fluorescent, but free guanine and free or bound guanosine are not. The single turnover numbers (k_3) for HsPNP, E:R-PNP and BtPNP increased monotonically with increasing temperature (Figure 5). BtPNP showed the highest rates (k_3) at all temperatures followed by E:R-PNP, while HsPNP showed the lowest rates. The differences increased at physiological temperature (Figure 5 and Table 3). For example, the single turnover numbers for BtPNP were 316 and 940 s^{-1} at 25 and 37 °C, respectively, in comparison with 214 and 840 s^{-1} for E:R-PNP, and 154 and 540 s^{-1} for HsPNP (Table 3). Analysis of the temperature dependences of the single turnover number (k_3) according to Arrhenius and Eyring equations for the three species of PNP showed linear increases of the ln(k) or ln(k/T) values with increasing temperature (Figure 5). Different activation enthalpies ($\Delta H^{\ddagger}$) and activation entropies ($\Delta S^{\ddagger}$) for the conversion of PNP•guanosine•PO_4 into PNP•guanine•R-1-P are demonstrated by different slopes and y-intercepts for the three PNPs (Figures 3 and 5, Table 3).

Activation entropy is a system parameter composed of several components including (1) the spatial freedom of the substrate within the enzyme active site, (2) differences of the degree of freedom of the catalytic site residues of the protein, and (3) solvent reorganization (*21*, *22*). For E:R-PNP, the remote mutations (≥25 Å from the catalytic site) resulted in an increase of the activation enthalpy ($\Delta H^{\ddagger}$), the activation entropy ($T\Delta S^{\ddagger}$), and the activation energy (E_a) compared to that for HsPNP (Table 3). The single turnover rates (k_3) for E:R-PNP were 1.5-fold greater than for HsPNP. A favorable entropic term offsets the less favorable enthalpic component, and accounts for an increase in k_3 from 154 to 214 s^{-1} at 25 °C (Table 3). This observation appears to be unusual relative to other examples in the literature, where a favorable entropy component compensates for unfavorable activation enthalpy and activation energy terms (*21*−*25*). Thus, the proposed enhanced mobility and dynamics of the F159 loop of subunit C in turn enhances the geometry and the dynamics of the active site residues (H257, F200, and Y88; subunit A) to increase the probability of forming the transition state for E:R-PNP (Figure 4). The enhanced activation entropy is characteristic of an altered transition-state structure, and the difference is shown to be the degree of participation of the nucleophile (described in ref *34*). The 2-fold difference in single turnover rates (k_3) between BtPNP and HsPNP is also explained by the differences in $\Delta H^{\ddagger}$, E_a, and $T\Delta S^{\ddagger}$ (Table 3). In this case, the enthalpic term diminished to mask the entropic term, resulting in 2-fold faster enzyme. From the point of view of the transition-state structure, BtPNP forms an earlier transition state relative to HsPNP as a result of a more highly activated leaving group and an early ribooxacarbenium ion transition-state structure.

Enzymatic enthalpy/entropy compensation is not fully understood (*26*−*28*). The contribution of differential entropic activation has not been fully explained in protein modeling studies due to its complexity, although suggestions of how to handle this component have been proposed (*28*−*31*). However, these parameters are simplified by comparing thermodynamic parameters for closely related PNPs catalyzing the same reaction. Here, the entropic contributions are most likely to result from altered dynamic modes leading to transition-state formation.

Computational analysis of E:R-PNP suggested a dynamic connection path whereby the remote mutations affect vibrational interactions transmitted into the active site.[2] The power spectra of E:R-PNP complexed with the transition-state analogue (ImmG) and phosphate showed a correlation between the vibration of O5′−N4′ and H257:ND1−ImmG:O5′, consistent with the dynamic coupling of the group and in turn contributing to catalysis (*32*, *33*). Enhanced dynamic coupling and enhanced activation entropy ($\Delta S^{\ddagger}$), together with the enhanced single turnover number caused by remote mutations in E:R-PNP, establish the mechanism in which remote dynamics are coupled into the catalytic site of human PNP.

REFERENCES

1. Schramm, V. L. (2005) Enzymatic transition states: thermodynamics, dynamics and analogue design, *Arch. Biochem. Biophys. 433*, 13−26.

2. Stoeckler, J. D., Cambor, C., and Parks, R. E., Jr. (1980) Human erythrocytic purine nucleoside phosphorylase: reaction with sugar-modified nucleoside substrates, *Biochemistry 19*, 102−107.
3. Giblett, E. R., Ammann, A. J., Wara, D. W., Sandman, R., and Diamond, L. K. (1975) Nucleoside-phosphorylase deficiency in a child with severely defective T-cell immunity and normal B-cell immunity, *Lancet 1*, 1010−1013.
4. Duvic, M., Olsen, E. A., Omura, G. A., Maize, J. C., Vonderheid, E. C., Elmets, C. A., Shupack, J. L., Demierre, M. F., Kuzel, T. M., and Sanders, D. Y. (2001) A phase III, randomized, double-blind, placebo-controlled study of peldesine (BCX-34) cream as topical therapy for cutaneous T-cell lymphoma, *J. Am. Acad. Dermatol. 44*, 940−947.
5. Ealick, S. E., Babu, Y. S., Bugg, C. E., Erion, M. D., Guida, W. C., Montgomery, J. A., and Secrist, J. A., 3rd. (1991) Application of crystallographic and modeling methods in the design of purine nucleoside phosphorylase inhibitors, *Proc. Natl. Acad. Sci. U.S.A. 88*, 11540−11544.
6. Schramm, V. L. (2002) Development of transition state analogues of purine nucleoside phosphorylase as anti-T-cell agents, *Biochim. Biophys. Acta 1587*, 107−117.
7. Kline, P. C., and Schramm, V. L. (1993) Purine nucleoside phosphorylase. Catalytic mechanism and transition-state analysis of the arsenolysis reaction, *Biochemistry 32*, 13212−13219.
8. Lewandowicz, A., Ringia, E. A., Ting, L. M., Kim, K., Tyler, P. C., Evans, G. B., Zubkova, O. V., Mee, S., Painter, G. F., Lenz, D. H., Furneaux, R. H., and Schramm, V. L. (2005) Energetic mapping of transition state analogue interactions with human and *Plasmodium falciparum* purine nucleoside phosphorylases, *J. Biol. Chem. 280*, 30320−30328.
9. Lewandowicz, A., and Schramm, V. L. (2004) Transition state analysis for human and *Plasmodium falciparum* purine nucleoside phosphorylases, *Biochemistry 43*, 1458−1468.
10. Miles, R. W., Tyler, P. C., Furneaux, R. H., Bagdassarian, C. K., and Schramm, V. L. (1998) One-third-the-sites transition-state inhibitors for purine nucleoside phosphorylase, *Biochemistry 37*, 8615−8621.
11. Lewandowicz, A., Shi, W., Evans, G. B., Tyler, P. C., Furneaux, R. H., Basso, L. A., Santos, D. S., Almo, S. C., and Schramm, V. L. (2003) Over-the-barrier transition state analogues and crystal structure with *Mycobacterium tuberculosis* purine nucleoside phosphorylase, *Biochemistry 42*, 6057−6066.
12. Narayana, S. V. L., Bugg, C. E., and Ealick, S. E. (1997) Refined structure of purine nucleoside phosphorylase at 2.75 Å resolution, *Acta Crystallogr. D53*, 131−142.
13. Kim, B. K., Cha, S., and Parks, R. E., Jr. (1968) Purine nucleoside phosphorylase from human erythroyctes. II. Kinetic analysis and substrate-binding studies, *J. Biol. Chem. 243*, 1771−1776.
14. Kicska, G. A., Tyler, P. C., Evans, G. B., Furneaux, R. H., Kim, K., and Schramm, V. L. (2002) Transition State Analogue Inhibitors of Purine Nucleoside Phosphorylase from *Plasmodium falciparum*, *J. Biol. Chem. 277*, 3219−3225.
15. Rinaldo-Matthis, A., Wing, C., Ghanem, M., Deng, H., Wu, P., Gupta, A., Tyler, P. C., Evans, G. B., Furneaux, R. H., Almo, S. C., Wang, C. C., and Schramm, V. L. (2007) Inhibition and Structure of *Trichomonas vaginalis* Purine Nucleoside Phosphorylase with Picomolar Transition State Analogues, *Biochemistry 46*, 659−668.
16. Singh, V., Evans, G. B., Lenz, D. H., Mason, J. M., Clinch, K., Mee, S., Painter, G. F., Tyler, P. C., Furneaux, R. H., Lee, J. E., Howell, P. L., and Schramm, V. L. (2005) Femtomolar transition state analogue inhibitors of 5′-methylthioadenosine/S-adenosylhomocysteine nucleosidase from *Escherichia coli*, *J. Biol. Chem. 280*, 18265−18273.
17. Kicska, G. A., Tyler, P. C., Evans, G. B., Furneaux, R. H., Shi, W., Fedorov, A., Lewandowicz, A., Cahill, S. M., Almo, S. C., and Schramm, V. L. (2002) Atomic dissection of the hydrogen bond network for transition-state analogue binding to purine nucleoside phosphorylase, *Biochemistry 41*, 14489−14498.
18. Taylor Ringia, E. A., and Schramm, V. L. (2005) Transition states and inhibitors of the purine nucleoside phosphorylase family, *Curr. Top. Med. Chem. 5*, 1237−1258.
19. Dlugosz, M., Bzowska, A., and Antosiewicz, J. M. (2005) Stopped-flow studies of guanine binding by calf spleen purine nucleoside phosphorylase, *Biophys. Chem. 115*, 67−76.
20. Wielgus-Kutrowska, B., Bzowska, A., Tebbe, J., Koellner, G., and Shugar, D. (2002) Purine nucleoside phosphorylase from Cellulomonas sp.: physicochemical properties and binding of substrates determined by ligand-dependent enhancement of enzyme intrinsic fluorescence, and by protective effects of ligands on thermal inactivation of the enzyme, *Biochim. Biophys. Acta 1597*, 320−334.
21. Ottosson, J., Fransson, L., and Hult, K. (2002) Substrate entropy in enzyme enantioselectivity: an experimental and molecular modeling study of a lipase, *Protein Sci. 11*, 1462−1471.
22. Ottosson, J., Rotticci-Mulder, J. C., Rotticci, D., and Hult, K. (2001) Rational design of enantioselective enzymes requires considerations of entropy, *Protein Sci. 10*, 1769−1774.
23. Jonsson, Wehtje, E., Adlercreutz, P., and Mattiasson, B. (1999) Thermodynamic and kinetic aspects on water vs. organic solvent as reaction media in the enzyme-catalysed reduction of ketones, *Biochim. Biophys. Acta 1430*, 313−322.
24. Verheyden, G., Matrai, J., Volckaert, G., and Engelborghs, Y. (2004) A fluorescence stopped-flow kinetic study of the conformational activation of α-chymotrypsin and several mutants, *Protein Sci. 13*, 2533−2540.
25. Jensen, M. P., Payeras, A. M., Fiedler, A. T., Costas, M., Kaizer, J., Stubna, A., Munck, E., and Que, L., Jr. (2007) Kinetic analysis of the conversion of nonheme (alkylperoxo)iron(III) species to iron(IV) complexes, *Inorg. Chem. 46*, 2398−2408.
26. Battistuzzi, G., Borsari, M., Di Rocco, G., Ranieri, A., and Sola, M. (2004) Enthalpy/entropy compensation phenomena in the reduction thermodynamics of electron transport metalloproteins, *J. Biol. Inorg. Chem. 9*, 23−26.
27. Cornish-Bowden, A. (2002) Enthalpy-entropy compensation: a phantom phenomenon, *J. Biosci. 27*, 121−126.
28. Sharp, K. (2001) Entropy-enthalpy compensation: fact or artifact?, *Protein Sci. 10*, 661−667.
29. Street, T. O., Bradley, C. M., and Barrick, D. (2005) An improved experimental system for determining small folding entropy changes resulting from proline to alanine substitutions, *Protein Sci. 14*, 2429−2435.
30. Vaz, D. C., Rodrigues, J. R., Sebald, W., Dobson, C. M., and Brito, R. M. (2006) Enthalpic and entropic contributions mediate the role of disulfide bonds on the conformational stability of interleukin-4, *Protein Sci. 15*, 33−44.
31. Villa, J., Strajbl, M., Glennon, T. M., Sham, Y. Y., Chu, Z. T., and Warshel, A. (2000) How important are entropic contributions to enzyme catalysis?, *Proc. Natl. Acad. Sci. U.S.A. 97*, 11899−11904.
32. Nunez, S., Antoniou, D., Schramm, V. L., and Schwartz, S. D. (2004) Promoting vibrations in human purine nucleoside phosphorylase. A molecular dynamics and hybrid quantum mechanical/molecular mechanical study, *J. Am. Chem. Soc. 126*, 15720−15729.
33. Murkin, A. S., Birck, M. R., Rinaldo-Matthis, A., Shi, W., Taylor, E. A. S. C. A., and Schramm, V. L. (2007) Neighboring group participation in the transition state of human purine nucleoside phosphorylase, *Biochemistry 46*, 5038−5049.
34. Luo, M., Li, L., and Schramm, V. L. (2008) Remote mutations alter transition-state structure of human purine nucleoside phosphorylase, *Biochemistry 47*, 2565−2576.

BI702132E